Dual-energy computed tomography: new technology for metal artifacts reduction

Exequiel Reynoso, Patricia Carrascosa, Carlos Capuñay, Alejandro Rasumoff, Javier Vallejos, Jimena Carpio, Karen Lago

Diagnóstico Maipú, Buenos Aires

Received on November 26th, 2015; accepted after evaluation on September 23rd, 2016. • EXEQUIEL REYNOSO, MD • reynoso.exequiel@gamail.com

Abstract

Introduction: Our goal was to explore the value of dual-energy CT scanning by gemstone spectral images and that of a program aimed at reducing metallic artifacts (MARS), so as to evaluate periprosthetic tissues and the diagnostic interpretability of conditions associated with implants.

Materials and Methods: We compared bone, soft tissues and fat density at periprosthetic tissues level with that in control tissues with no implant, using a high definition dual-energy CT scanner both in conventional polychromatic images and in virtual monochromatic images with MARS, in 80 patients with metallic prosthesis in different areas of their skeletal system. We assessed the quality of the image and the diagnostic interpretability using the Likert scale.

Results: In polychromatic images there were significant differences in the periprosthetic area in the three types of tissues as compared to the control subjects ($p<0.0001$); there were no significant differences while using virtual monochromatic spectral images-MARS (bone $p=0.053$, soft tissues $p= 0.32$ and fat $p= 0.13$), with more resemblance to normal tissues. Noise levels were significantly higher in polychromatic images ($p<0.0001$) than in virtual monochromatic spectral images-MARS. We considered as non-interpretable ones all the periprosthetic regions in polychromatic images and 11 (9%) in virtual monochromatic spectral images-MARS. There were no significant differences in radiation doses as compared to the control group ($p=0.21$).

Conclusions: Dual-energy CT scan can reduce periprosthetic artifacts increasing significantly the potential for tissue identification and the diagnostic interpretability of likely conditions associated with implants.

Key words: Implant; prosthesis; spectral images, diagnosis

Level of evidence: II

Tomografía computarizada de doble energía: nueva tecnología para la reducción de artefactos de metal

Resumen

Introducción: El objetivo fue explorar la utilidad de la tomografía computarizada de doble energía mediante tecnología de imágenes espectrales *gemstone* y de un programa destinado a la reducción de artefactos de metal (MARS), para evaluar tejidos periprotésicos, y la interpretabilidad diagnóstica de patologías relacionadas con implantes.

Conflict of interests: The authors have reported none.

http://dx.doi.org/10.15417/572

Materiales y Métodos: Se comparó la densidad ósea, de partes blandas y de grasa en el tejido periprotésico y en tejido de control sin implante, utilizando un escáner de alta definición de tomografía computarizada de doble energía tanto en imágenes policromáticas convencionales, como en monocromáticas virtuales con MARS, en 80 pacientes con prótesis metálicas en diversas regiones musculoesqueléticas. Se valoró la calidad de imagen y la interpretabilidad diagnóstica mediante la escala de Likert.
Resultados: Con imágenes policromáticas hubo diferencias significativas entre el área periprotésica en los tres tejidos respecto a los controles (p <0,0001); sin diferencias significativas utilizando imágenes espectrales monocromáticas virtuales-MARS (hueso p = 0,053, partes blandas p = 0,32 y grasa p = 0,13), con más similitud con el tejido normal. Los niveles de ruido fueron significativamente mayores con imágenes policromáticas (p <0,0001) que con imágenes espectrales monocromáticas virtuales-MARS. Se consideraron no interpretables todas las regiones periprotésicas en las imágenes policromáticas y 11 (9%) en las imágenes espectrales monocromáticas virtuales-MARS. No hubo diferencias significativas en la dosis de radiación comparada con la del grupo control (p = 0,21).
Conclusiones: La tomografía computarizada de doble energía puede reducir los artefactos periprotésicos, logrando un significativo incremento en la capacidad de identificar tejidos y la interpretabilidad diagnóstica de posibles patologías relacionadas con implantes.

Palabras clave: Implante; prótesis; imágenes espectrales; diagnóstico.
Nivel de Evidencia: II

Introduction

CT scanning plays a key role in the assessment of the patients with metallic prosthesis, and it is crucial for these patients' post-operative follow-up and the management of potential complications. However, we are still to overcome one of the main drawbacks associated with these techniques—the periprosthetic artifacts that stem from metallic implants.[1]

In this context, thanks to the recent development of dual-energy CT scanning (DECT) it is possible to synthesize virtual monochromatic spectral images (VMSIs) which can show the object as if it were being studied using conventional CT scanning (simple energy CT scanning) but that can also reduce periprosthetic artifacts, thus improving the intefaz between tissues.[2-7]

Moreover, other approaches aimed at dealing with these problems have been developed, such as algorithms of adaptative statistical iterative reconstruction (ASIR) [8-10] and metal artifact reduction software (MARS).[11,12]

There is no research that reports the combined performance of these techniques in the quantitative evaluation of periprosthetic tissues using densitometric figures. Therefore, we explored the value of DECT of unique source in association with MARS and ASIR algorithms developed using the same technology. Our goal was to evaluate artifact reduction in the periprosthetic area and the diagnostic interpretability of potential complications related to the implants.

Materials and Methods

Design and study population

We recruited prospectively consecutive patients that had been referred for post-operative evaluation of metallic prosthesis in different anatomic areas of their skeletal system, between March 2013 and June 2015.

The images were taken at least 15 days after the surgical procedure had taken place, as it was required and according to general indications. We excluded women that were potentially or effectively pregnant, and patients with BMI >32kg/m^2.

Images taking

Patients were assessed using a dual-energy-detector 64-slide CT scanner (Discovery™, HD 750, GE Healthcare, Milwaukee, USA) which allows VMSIs to be generated for further analysis. Data processing was carried out off-line at a work station equipped with a specific program available on the market (AW 4.6, GE Healthcare, Milwaukee, USA).

The images initially taken with this type of CT scanners offer, apart from monochromatic information (VMSIs), information about polychromatic images (PI) similar to that gotten using simple-energy conventional CT scanners, and this way it is possible to do a comparable analysis; therefore, it was used instead, so as not to have to evaluate the patients again (Figure 1). [4,13]

In all cases we carried out reconstruction to get VMSIs with high energetic levels (140 keV) combined with MARS developed using the same technology (Figure 1), since VMSIs with higher energetic levels have been found to be the ones that ameliorate metallic artifacts better. [6,14,15]Moreover, we applied ASIR systematically to sheer data gotten at 50%, since this technology has been found to improve image quality and thus promote the use of lower radiation doses. [8-10]

Quantitative analysis of the images

Images data were analyzed at the same work station that images were processed at. We evaluated the detection of three basic types of tissues adjacent to the prosthesis, in the artifacts area, by means of specific regions destined to estimate figures in Hounsfield units: bone, soft tissues and fat (Figure 1). Soft tissues were thought of as represented by muscle tissue, fiber-scar tissue, parenchyma tissue and others of similar density such as inflammatory tissue.

Periprosthetic artifacts were defined as the ones that arise when X-ray beams or parts of X-ray beams go through specific objects, such as metals, and behave differently when they go through the same objects in different positions of the X-ray tube, what shows as black (low attenuation component) and bright (high attenuation component) stripes.[4] Periprostehtic assessment was carried out in the areas of the greatest artifact, defined as those ones where the lowest attenuation component is projected (black stripes) (Figure 1). Likewise, we evaluated in the same way the standard deviation of every figure to calculate the image noise and the signal/noise ratio.

Every patient was subject to this procedure focusing on the same anatomic area for the three types of tissues, both in PIs and the VMSI-MARS. The same procedure was followed in the same patients on their contralateral side with no prosthesis (control group). When the patients had bilateral prosthesis (cases of hip bilateral replacement) or when it was not possible to get data out of the contralateral side, the assessment was carried out in the nearby area that showed characteristics similar to those ones of the tissues unaffected by the artifact (such as the pelvis). When the spine was involved, we assessed the nearby vertebral levels that had neither prosthesis nor artifacts.

We also evaluated the effective radiation doses administered under the correction factor for every anatomic area, which was suggested by international standards.[16] As control group for this analysis, we used a group made up of the same number of patients matched by gender and age, who were evaluated for other reasons in the same anatomic areas using the same CT scanner with conventional PIs.

Qualitative analysis of the images

We assessed the image quality of every type of tissue within the artifact area, together with the general diagnostic interpretability of the study (Figure 2).

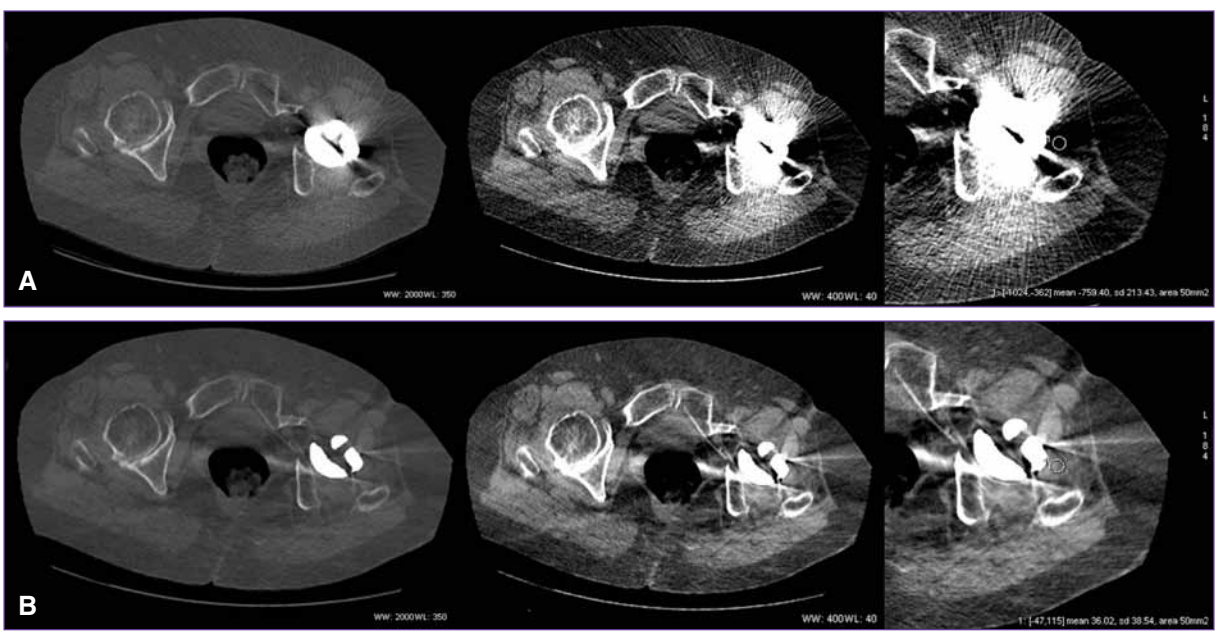

Figure 1. Seventy-one year-old male with left total hip replacement. Transverse section dual-energy CT scan. **A.** Polychromatic images with window adjustment for bone tissue (first upper panel) and soft tissues (second upper panel) evaluation. Fifty mm^2 focused region to evaluate tissue density within the low attenuation component of the artifact associated with the implant (third upper panel). **B.** Same procedure with spectral monochromatic images (VMSI-MARS). Note the significant reduction in artifacts.

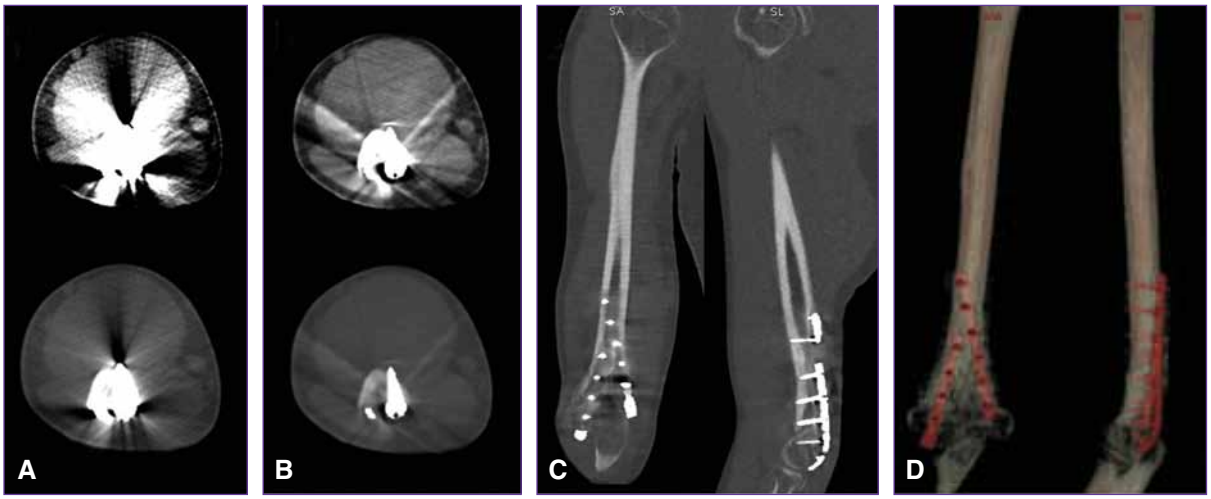

Figure 2. Twenty-six year-old male with right distal humeral fracture treated with fixation plate and screws. Double-energy CT scan. **A.** Conventional transverse section images showing important artifacts with periprosthetic deterioration that hampers the evaluation of the adjacent tissues with evaluation window for both soft tissues (upper panel) and bone tissues (lower panel). **B.** Virtual monochromatic transverse images with MARS which reduce artifacts significantly, what allows the observer to improve the evaluation of periprosthetic bone tissues (lower panel), soft tissues and fat tissue (upper panel). C. Tridimensional (D) coronal and sagittal monochromatic images which allow the observer to evaluate better the position of the fixation plate and screws.

Image quality was evaluated by a six-item Likert-type scale (Table 1): 1) Total invisibility of the structures darkened by the artifacts, 2) severe artifacts with insufficient identification of the anatomic structures, 3) moderate artifacts with insufficient identification of the structures surrounding the prosthesis, 4) moderate artifacts that allow the observer to identify the anatomic structures and the tissues, 5) mild artifacts with adequate identification of the anatomic structures and the tissues, 6) normal tissues with no artifacts. We always used the same width and the pre-established window level to visualize the bone tissue (level=350, width=200) and soft tissues (level=40, width=400) in the same transverse image both in PIs and in VMSI-MARS.

Diagnostic interpretability was determined by agreement by two experimented observers (CC and ER) who used a five-item Likert-type scale evaluating the potential to identify images considered abnormal (Table 1) according to the observer's criteria and visualizing the whole exam: 1) total invisibility of the structures darkened by the artifacts, 2) image quality deteriorated by the artifacts that hamper appropriate evaluation, 3) sub-optimal; reduction of image quality, which is adequate anyway to get a diagnostic impression, 4) good; mild artifacts, mild image noises with adequate differentiation between normal and abnormal structures, 5) excellent; absent or minimal artifacts with excellent delimitation of the periprosthetic anatomic structures and normal structures, with no drawbacks to diagnostic specifications, similar to images with no prosthesis.

As pre-established post hoc evaluation we carried out an analysis specified by the different anatomic areas being

Table 1. Analysis of the image quality in every tissue being studied, diagnostic interpretability and non-diagnostic studies rates

	Polychromatic image	VMSI-MARS	p
Bone	1.58 ± 0.8	3.39 ± 0.9	<0.0001
Soft tissues	1.38 ± 0.7	3.55 ± 1.0	<0.0001
Fat	1.80 ± 0.9	3.70 ± 1.0	<0.0001
Diagnostic interpretability	1.08 ± 0.3	3.35 ± 0.7	<0.0001
Non-diagnostic (%)	80 (100%)	11 (9%)	<0.0001

VMSIs = virtual monochromatic spectral images; MARS = *metal artifact reduction software.*
Comparison by Wilcoxon-signed rank test

studied, grouped in five regions: hip, knee, long bones, spine and other regions.

All the procedures were followed as established by the Ethical Standards set by the Institutional Research Committee in compliance with the 1964 Helsinki Declaration and further amendments. We had every person included in the study signing the written informed consent.

Statistical analysis

Categorical variables were expressed as calculations and percentages, whereas continuous variables were expressed as average ± standard deviation (SD) in the case of normal distribution and as median with interquartile range (IQR) for non-normal distribution variables. Non-parametric comparisons between groups were made using the Wilcoxon-signed rank test. The level of statistical signification was established as $p<0.05$. We used the 22.0 version SPSS statistical program (Chicago, Illinois, USA).

Results

Out of the 87 patients initially recruited, we excluded four because the parameters of examination were different from the pre-established ones and three because the reconstruction and processing parameters were inadequate. Therefore, 80 patients followed the whole protocol and were included in the analysis.

Age median was 63.5 (IQR= 41.0-73.8), and 32 (40%) patients were males. The examined regions were hips=23 (29%); knees=14 (18%); the spine=16 (20%); long bones= eight (10%; humerus, femur, ulna and radius, tibia and fibula) and other regions=19 (24%; shoulder, elbow, hand and wrist, ankle and foot, collar bone, breast bone, ribs and skull).

Quantitative analysis of the images

Bone tissue: In all the regions being studied, we found significant differences in the figures in periprosthetic Hounsfield units as compared to the control (contralateral) tissues in the PIs reconstructions ($p<0.0001$), whereas we did not find significant differences in VMSI-MARS ($p = 0.053$). Image noise was lower in VMSI-MARS than PIs (Table 2).

Soft tissues: We also found significant differences in the attenuation levels between prosthesis and control subjects in the PIs group ($p <0.0001$), with no differences in the VMSI-MARS group ($p = 0.32$). Image noise was also lower in VMSI-MARS than in PIs (Table 3, Figure 1).

Fatty tissue: We found significant differences in the levels of density between prosthesis and control subjects in the PIs group ($p<0.0001$), with no significant differences in the VMSI-MARS group ($p = 0.13$). Image noise was also lower in VMSI-MARS (Table 4).

Table 2. Bone tissue analysis

	Polychromatic image	VMSI-MARS	p
Prosthesis (bone)			
Density (HUs)	-262.2 (-519.9; -85.5)	88.2 (55.8; 176.3)	<0.0001
Noise (SD)	131.5 (79.4; 205.8)	39.7 (28.1; 72.2)	<0.0001
Signal/noise ratio	-2.0 (-3.7; -0.9)	2.4 (1.2; 3.4)	<0.0001
Control (bone)			
Density (HUs)	193.5 (143.1; 266.5)	110.2 (86.9; 155.4)	<0.0001
Noise (SD)	50.0 (39.5; 62.4)	38.3 (29.8; 53.1)	<0.0001
Signal/noise ratio	3.8 (2.6; 5.2)	3.0 (2.1; 3.8)	0.001
p values for the differences between periprosthetic tissues and control subjects			
Density (HUs)	<0.0001	0.053	
Noise (SD)	<0.0001	0.37	
Signal/noise ratio	<0.0001	0.10	

VMSIs = virtual monochromatic spectral images; MARS= *metal artifact reduction software;* HUs = Hounsfield units; SD = average density standard deviation. Comparison by Wilcoxon-signed rank test

Table 3. Soft tissues analysis

	Polychromatic image	VMSI-MARS	p
Prosthesis (bone)			
Density (HUs)	-250.2 (-434.2; -147.0)	47.5 (28.5; 66.6)	<0.0001
Noise (SD)	69.5 (43.8; 110.0)	20.2 (14.1; 30.1)	<0.0001
Signal/noise ratio	-4.0 (-6.0; -2.2)	2.2 (1.0; 3.7)	<0.0001
Control (bone)			
Density (HUs)	50.0 (38.8; 59.9)	43.2 (37.5; 49.9)	<0.0001
Noise (SD)	17.0 (12.3; 24.0)	12.8 (10.4; 18.3)	<0.0001
Signal/noise ratio	2.6 (1.7; 4.3)	3.2 (2.2; 4.5)	0.17
p values for the differences between periprosthetic tissues and control subjects			
Density (HUs)	<0.0001	0.32	
Noise (SD)	<0.0001	<0.0001	
Signal/noise ratio	<0.0001	<0.0001	

VMSIs = virtual monochromatic spectral images; MARS= *metal artifact reduction software;* HUs = Hounsfield units; SD = average density standard deviation. Comparison by Wilcoxon-signed rank test

Figure 3. Eighty-seven year-old male with left proximal humeral fracture after undergoing surgery. Dual-energy CT scan. **A.** Polychromatic transverse images showing periprosthetic artifacts that hamper seriously the evaluation of the shoulder. **B and C.** Transverse and oblique coronal virtual monochromatic images with MARS which reduce artifacts significantly and evidence the fracture with epiphyseal detachment and signs of bone resorption and granulation/fibrosis tissues associated. **D.** Tridimensional images generated by the virtual monochromatic data that show clearly the fracture and the position of the prosthesis.

Tabla 4. Fatty tissue analysis

	Polychromatic image	VMSI-MARS	p
Prosthesis (bone)			
Density (HUs)	-218.8 (-317.7; -167.3)	-74.8 (-90.8; -59.2)	<0.0001
Noise (SD)	32.2 (25.4; 69.3)	16.3 (12.4; 23.7)	<0.0001
Signal/noise ratio	-5.5 (-8.8; -3.6)	-4.6 (-6.3; -2.9)	0.001
Control (bone)			
Density (HUs)	-98.3 (-111.3; -84.7)	-78.8 (-85.2; -71.0)	<0.0001
Noise (SD)	16.0 (12.7; 21.3)	12.3 (10.0; 16.7)	0.002
Signal/noise ratio	-6.0 (-7.6; -4.4)	-6.1 (-7.8; -4.7)	<0.001
p values for the differences between periprosthetic tissues and control subjects			
Density (HUs)	<0.0001	0.13	
Noise (SD)	<0.0001	<0.0001	
Signal/noise ratio	0.02	<0.0001	

VMSIs = virtual monochromatic spectral images; MARS= *metal artifact reduction software;* HUs= Hounsfield units; SD = average density standard deviation. Comparison by Wilcoxon-signed rank test.

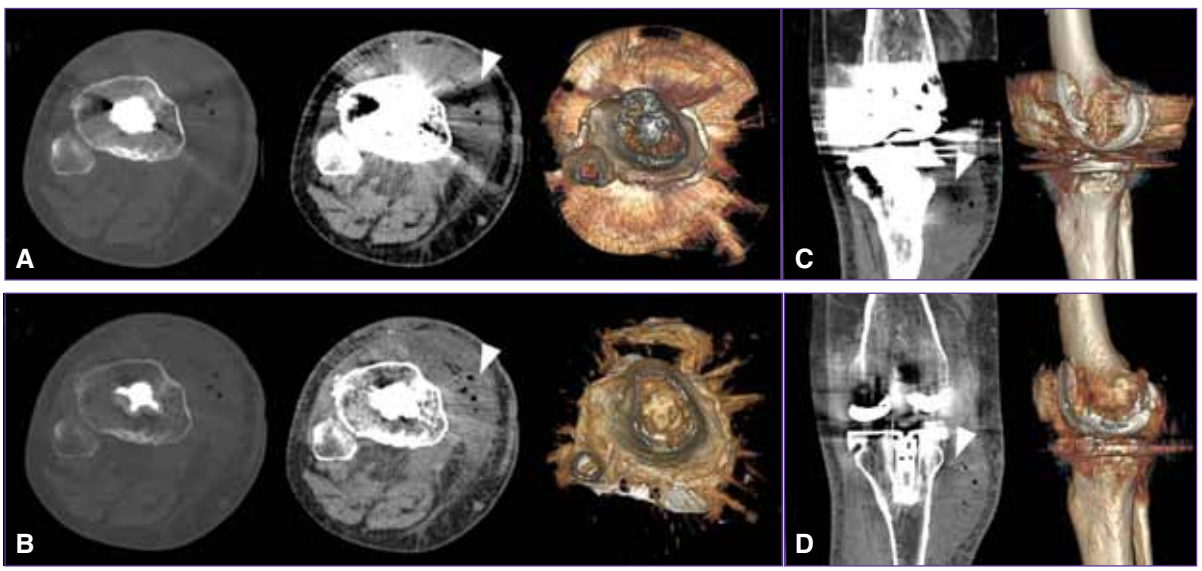

Figure 4. Seventy year-old male with right knee arthroplasty. Dual-energy CT scan. **A.** Conventional polychromatic images with window adjustment for bone (first panel) and for soft tissues (second panel) evaluation which show an artifact (arrowhead) that deteriorates the image on the medial anterior-lateral area of the joint. There is also a lower sight of a tridimensional image (third panel) affected by the artifacts. **B.** Important reduction of the artifacts which evidence a periarticular collection with small images of air density, probably caused by an infectious/inflammatory disorder. **C.** Polichromatic and tridimensional coronal image that shows the artifacts on the aforementioned collection (arrowhead). **D.** Monochromatic coronal image with MARS and resultant tridimensional image which also show sheer reduction of the artifacts and improvement in the quality of the image.

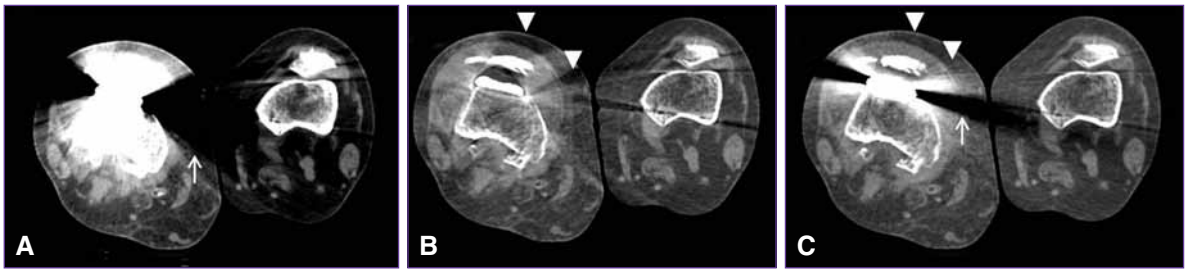

Figure 5. Sixty-five year-old female with right knee arthroplasty. Transverse section dual-energy CT scan. **A.** Polychromatic image with window adjustment for soft tissues evaluation which shows an important artifact that deteriorates the quality of the image (white arrow). **B.** Same section level showing a spectral monochromatic image with MARS with significant reduction of artifacts; there is a secondary artifact (arrowhead) on the anterior area of the joint. **C.** Virtual monochromatic image without MARS which also shows reduction of artifacts (although to a lesser extent), with no additional artifacts.

Qualitative analysis of the images

Image quality evaluation

Image quality was significantly better in VMSI-MARS reconstructions, in the bone tissue (PIs 1.58 ± 0.8 and VMSI-MARS 3.39 ± 0.9; p <0.0001), in soft tissues (PIs 1.38 ± 0.7 and VMSI-MARS 3.55 ± 1.0; p <0.0001) and the fatty tissue (PIs 1.80 ± 0.9 and VMSI-MARS 3.70 ± 1.0; p <0.0001) (Table 1, Figure 3).

Evaluation of diagnostic interpretability

All the cases evaluated by PIs reconstructions were considered to be non-interpretable as compared to only 11 (9%) cases in VMSI-MARS (p <0.0001) (Table 1, Figure 4).

Effective radiation doses

We did not find significant differences in the effective radiation doses between the population being studied and the control subjects that were studied using simple-energy conventional images (PIs) [median 4.7 mSv, IQR 0.50; 7.44) vs. 3.6 mSv (IQR 0.30; 6.54); p = 0.21].

Discussion

Our piece of research describes the potential of the DECT technology to reduce the artifacts related to metallic implants both in subjective and objective ways, with levels of periprosthetic tissues density that can be compared to those of the normal contralateral tissues in the same patient. Our results suggest that in the periprosthetic bone tissue, soft tissues and fatty tissue, VMSI-MARS reduce artifacts significantly as compared to the images taken with simple-energy conventional CT scanners (Figures 2-4), with no significant differences in attenuation levels with respect to control subjects in either of the tissues being studied (Tables 2-4). It is worth mentioning that this strategy does not imply any increase in radiation doses.

Lee et al. described in 26 subjects that VMSI-MARS are particularly sensitive to the makeup, the form and the size of the prosthesis, what also can have an influence on the quality of the image;[14] these facts were also reported by other researchers that used similar technological devices. [6,7,12,15,17,18] We found in some specific anatomic areas mild heterogeneities in the periprothetic tissues in regions other than the artifact original ones that we called "secondary artifacts" (Figure 5). One of the advantages of the dual-energy system is the possibility to get VMSI without MARS, what has also proved to reduce the original artifacts seen with PIs with no secondary artifacts as by-products; moreover, it offers VMSI-MARS at the same time (Figure 5). [3,4,6,7,13] This way, it would be possible to get an incremental effect for the patient's general evaluation (diagnostic interpretability) because the observer has access to all the examination data available, something which is key for the post-operative evaluation of patients with potential complications associated with the implant, such as aseptic loosening, bone resorption or osteolysis, infection, dislocation and periprosthetic fracture.[19] In this context, diagnostic impression was better using VMSI-MARS than PIs—only 11% of the patients with VMSI-MARS had insufficient data for diagnosis, whereas no periprosthetic tissues with PIs were considered to be interpretable.

Limitations

It is worth mentioning some limitations. We included neither surgical nor arthroscopic data, nor did we study the artifact variability related to the material, the size and the surface of the prosthesis; we did not study the different energetic levels within the DECT system either. However, we did take into account previous reports on the subject.

Conclusions

In this prospective study, DECT technology proved to be able to reduce metallic artifacts and improve diagnostic interpretability of bone and joint periprosthetic tissues as compared to conventional images.

Bibliography

1. Barrett JF, Keat N. Artifacts in CT: recognition and avoidance. *Radiographics* 2004;24:1679-1691.
2. Matsumoto K, Jinzaki M, Tanami Y, Ueno A, Yamada M, Kuribayashi S. Virtual monochromatic spectral imaging with fast kilovoltage switching: improved image quality as compared with that obtained with conventional 120-kvp CT. *Radiology* 2011;259:257-262.
3. Bamberg F, Dierks A, Nikolaou K, Reiser MF, Becker CR, Johnson TR. Metal artifact reduction by dual energy computed tomography using monoenergetic extrapolation. *Eur Radiol* 2011;21:1424-1429.
4. Pessis E, Campagna R, Sverzut JM, Bach F, Rodallec M, Guerini H, et al. Virtual monochromatic spectral imaging with fast kilovoltage switching: reduction of metal artifacts at CT. *Radiographics* 2013;33:573-583.
5. Mangold S, Gatidis S, Luz O, Konig B, Schabel C, Bongers MN, et al. Single-source dual-energy computed tomography: use of monoenergetic extrapolation for a reduction of metal artifacts. *Invest Radiol* 2014;49:788-793.
6. Wang Y, Qian B, Li B, Qin G, Zhou Z, Qiu Y, et al. Metal artifacts reduction using monochromatic images from spectral CT: Evaluation of pedicle screws in patients with scoliosis. *Eur J Radiol* 2013;82:e360-366.
7. Meinel FG, Bischoff B, Zhang Q, Bamberg F, Reiser MF, Johnson TR. Metal artifact reduction by dual-energy computed tomography using energetic extrapolation: A systematically optimized protocol. *Invest Radiol* 2012;47:406-414.
8. Nakamoto A, Kim T, Hori M, Onishi H, Tsuboyama T, Sakane M, et al. Clinical evaluation of image quality and radiation dose reduction in upper abdominal computed tomography using model-based iterative reconstruction; comparison with filtered back projection and adaptive statistical iterative reconstruction. *Eur J Radiol* 2015;84:1715-1723.
9. Morsbach F, Bickelhaupt S, Wanner GA, Krauss A, Schmidt B, Alkadhi H. Reduction of metal artifacts from hip prostheses on CT images of the pelvis: Value of iterative reconstructions. *Radiology* 2013;268:237-244.
10. Zhu Z, Zhao XM, Zhao YF, Wang XY, Zhou CW. Feasibility study of using gemstone spectral imaging (GSI) and adaptive statistical iterative reconstruction (ASIR) for reducing radiation and iodine contrast dose in abdominal CT patients with high BMI values. *PloS One* 2015;10:e0129201.
11. Han SC, Chung YE, Lee YH, Park KK, Kim MJ, Kim KW. Metal artifact reduction software used with abdominopelvic dual-energy CT of patients with metal hip prostheses: assessment of image quality and clinical feasibility. *AJR Am J Roentgenol* 2014;203(4):788-795.
12. Schwahofer A, Bar E, Kuchenbecker S, Grossmann JG, Kachelriess M, Sterzing F. The application of metal artifact reduction (MAR) in CT scans for radiation oncology by monoenergetic extrapolation with a DECT scanner. *Z Med Phys* 2015;25(4): 314-325.
13. Jia Y, Zhang J, Fan J, Li C, Sun Y, Li D, Xiao X. Gemstone spectral imaging reduced artifacts from metal coils or clips after treatment of cerebral aneurysms: a retrospective study of 35 patients. *Br J Radiol* 2015;88(1055):2015-2022.
14. Lee YH, Park KK, Song HT, Kim S, Suh JS. Metal artefact reduction in gemstone spectral imaging dual-energy CT with and without metal artefact reduction software. *Eur Radiol* 2012;22:1331-1340.
15. Lewis M, Reid K, Toms AP. Reducing the effects of metal artefact using high keV monoenergetic reconstruction of dual energy CT (DECT) in hip replacements. *Skeletal Radiol* 2013;42:275-282.
16. European guidelines on quality criteria for computed tomography. Disponible en: http://www.Drs.Dk/guidelines/ct/quality/index.Htm. (Consulta: abril 2016).
17. Guggenberger R, Winklhofer S, Osterhoff G, Wanner GA, Fortunati M, Andreisek G, et al. Metallic artefact reduction with monoenergetic dual-energy CT: systematic ex vivo evaluation of posterior spinal fusion implants from various vendors and different spine levels. *Eur Radiol* 2012;22:2357-2364.
18. Schneider D, Apfaltrer P, Sudarski S, Nance JW, Jr., Haubenreisser H, Fink C, et al. Optimization of kiloelectron volt settings in cerebral and cervical dual-energy CT angiography determined with virtual monoenergetic imaging. *Acad Radiol* 2014;21: 431-436.
19. Liu PT, Pavlicek WP, Peter MB, Spangehl MJ, Roberts CC, Paden RG. Metal artifact reduction image reconstruction algorithm for CT of implanted metal orthopedic devices: a work in progress. *Skeletal Radiol* 2009;38:797-802.